Orbit-Related Variation in Spatial Resolution as a Source of Artifactual Defects in Thallium-201 SPECT

Piotr J. Maniawski, Hugh T. Morgan, and Frans J. Th. Wackers

Cardiovascular Nuclear Imaging Laboratory, Departments of Diagnostic Radiology (Nuclear Medicine) and Medicine (Cardiology), Yale University School of Medicine, New Haven, Connecticut and Picker International, Highland Heights, Ohio

The cause of 180-degree diametrical artifactual defects in clinical thallium-201 SPECT imaging was investigated using phantom simulation. This artifact was observed on SPECT images acquired with a "body contour" or "peanut" orbit. It was hypothesized that this artifact was caused by differences in spatial resolution that occur when the heart-to-detector distance changes employing noncircular orbits. To test this hypothesis, a series of planar static images of a normal cylindrical phantom was obtained at varying distances from the camera detector head. From these images, tomographic acquisition files were created that simulated tomographic data acquired with circular orbits and elliptical orbits. The reconstructed phantom short-axis slices showed no artifacts for *circular* orbits. However, for various *elliptical* orbits, significant regional nonuniformity, similar to the artifacts noted in patients, was observed. The degree of nonuniformity correlated with the long-short axis ratio of elliptical orbits ($r = 0.98$). In addition, circular orbits with the phantom in an *eccentric* position resulted in similar nonuniformities. It is concluded that a noncircular tomographic orbit can create characteristic artifacts on thallium-201 SPECT images. For rotational thallium 201 SPECT, a circular orbit with the heart in the center of rotation should be employed.

J Nucl Med 1991; 32:871-875

Thallium-201 (^{201}Tl) single-photon emission tomography (SPECT) has become a well established imaging modality for evaluation of the presence and extent of coronary artery disease. Compared to planar ^{201}Tl imaging, SPECT allows separation of superimposed myocardium and provides higher contrast images. Several recent reports suggested not only improved overall detection of coronary artery disease, but also improved localization of disease in specific coronary artery territories (*1-13*). However, most of these reports also indicate a certain loss of specificity with SPECT in comparison to planar imaging. Although this can be partially explained by "referral bias," ^{201}Tl SPECT unquestionably has greater potential for creation of artifacts than planar imaging.

Attenuation by the breast, diaphragm, and right ventricle can cause some of these artifacts. Other artifacts may be caused by patient motion and position (supine or prone), respiratory motion, and "upward creep" of the heart. Furthermore, instrumentation factors, such as center of rotation offset, flood nonuniformity, and nonlinearity of the detector, flaws in collimator construction, or mechanical inaccuracy of the gantry, should be considered as possible sources of artifacts on ^{201}Tl reconstructed slices (*14-16*).

In the present communication, we report and investigate another relatively frequent potential source for artifacts on SPECT images, which is related to the configuration of the orbit of the detector head around the heart. We observed repeatedly typical artifacts on tomographic ^{201}Tl-slices of normal subjects when an orbit was employed that followed the body contour (Fig. 1A-B). In these subjects, typical 180-degree diametrical defects were noted. We hypothesized that during acquisition at varying distances from the heart, varying spatial resolution created regional nonuniformity. Accordingly, we performed phantom studies to test this hypothesis.

METHODS

Phantom

A hollow cylindrical phantom (Fig. 2) was used in this study. This consisted of a solid inner cylinder (2.5 in. in diameter, 5 in. long) placed centrally within a larger hollow cylinder (3.5 in. in diameter, 5.25 in. long). The hollow space (width 0.5 in.) between the two cylinders was filled with a thoroughly mixed solution containing 500 μCi of ^{201}Tl. Thus, this phantom represented a simplified three-dimensional model of the left ventricular myocardium with homogeneous uptake of ^{201}Tl.

Received Jun. 1, 1990; revision accepted Nov. 2, 1990.

For reprints contact: Frans J. Th. Wackers, MD, Director, Cardiovascular Nuclear Imaging and Exercise Laboratories, Yale University School of Medicine, 333 Cedar St., TE-2, New Haven, CT 06510.

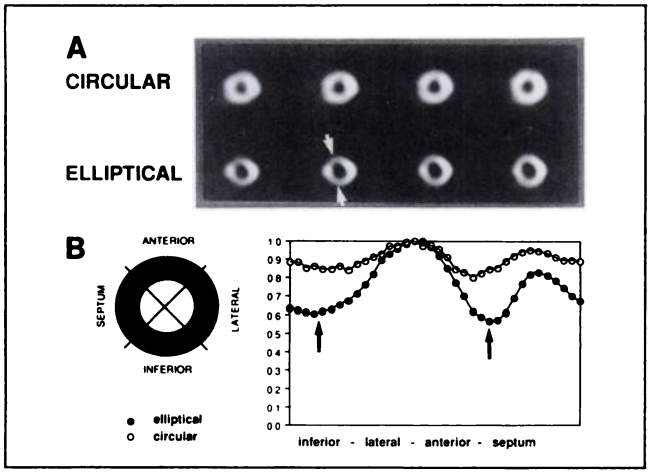

FIGURE 1. (A) Reconstructed short-axis slices of a normal subject imaged in the supine position. Top row: acquisition with a circular orbit. Bottom row: acquisition employing a "body contour" or elliptical orbit (see text). The images acquired with a circular orbit show homogeneous ^{201}Tl distribution. The images acquired with the elliptical orbit show inhomogeneous ^{201}Tl uptake and typical artifacts: 180-degree diametrical defects (arrows). (B) Circumferential profiles (10-degree angles) of the short-axis slices shown in Figure 1A (○ = circular orbit; ● = elliptical orbit). Data represent maximal counts in each angle from inferior wall counterclockwise. The distribution of counts after acquisition with an elliptical orbit shows marked inhomogeneity: two discrete areas (arrows) with approximately 40% relative reduction in count density. In contrast, the distribution of counts using a circular orbit is near homogeneous.

Data Acquisition

Imaging was performed using a large field of view rotating camera (model SX 300, Picker Intl., Highlands Heights, OH) equipped with a general-purpose low-energy parallel-hole collimator. The energy windows were set at 73 keV (40%) and 167 keV (20%). The camera was interfaced with a dedicated minicomputer (PCS PLUS, Picker Int., Highlands Heights, OH).

Planar static images of the phantom were acquired for 40 sec per image in 64 × 64 matrix. The count rate was similar to that usually obtained per 40 sec stop in a typical patient ^{201}Tl SPECT study.

To exclude the effect of artifacts that could be created by center of rotation offset, detector nonuniformity, collimator flaws, camera mechanics, and other technical factors, the acquisition of tomographic studies employing various orbits was simulated as outlined below.

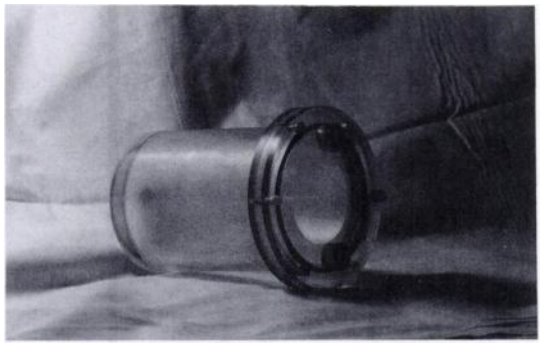

FIGURE 2. Cylindrical phantom. The hollow cylinder is filled with a homogeneous solution of ^{201}Tl.

Circular Orbit—Phantom at the Center of Rotation

The phantom was positioned in the center of the field of view. The camera head remained in the same position without rotation. Thirty-two static images were acquired at the same distance from the camera. A tomographic file for 180-degree angular sampling was created from these 32 images, simulating tomographic acquisition employing a circular orbit with a source of activity in the center of rotation. Eleven circular orbits with different radii were simulated by acquiring images at distances ranging from 17 cm to 35 cm.

Elliptical Orbits—Phantom at the Center of Rotation

The phantom was positioned in the center of the field of view. Thirty-two static images were acquired at *varying* distances from the detector. These images were acquired without rotation of the camera, by moving the camera head up and down. A tomographic file for 180-degree angular sampling was created from the images acquired with distances that satisfied an equation of an ellipse, thus simulating an elliptical orbit. Eleven simulated elliptical orbits were studied with varying short-to-long axis ratios. The short-axis of the ellipses was kept constant at 17 cm; the long-axis varied from 17 cm to 37 cm.

Circular Orbits—Phantom Positioned Out of the Center of Rotation

Simulation of a circular orbit with the phantom positioned "off center" was performed in three steps. First, the theoretical distances of the phantom to the camera were determined for each of the projections. They were calculated from the equation of a circle assuming that the center of the phantom was placed away from the center of the circle. Then, 32 static images were acquired at these distances by moving the camera head up and down. The phantom was positioned in the center of the field of view. Finally, using computer software all images were moved either to the left or right. This assured proper offset value for each of the projections. A tomographic file for 180-degree angular sampling was created from these images, thus simulating a circular orbit acquisition with a phantom positioned away from the center of rotation. The radius of the circular orbit was 25 cm. Eight different eccentric positions of the phantom were studied, ranging from 2 cm to 14 cm from the center of rotation.

Tomographic Reconstruction

Following the creation of tomographic files, reconstruction of short-axis slices (6 mm thickness) was performed using standard filtered backprojection. Images were filtered prior to reconstruction using an image-dependent Metz filter (*17*). No attenuation or scatter correction was performed.

Nonuniformity Measurement

To measure regional nonuniformity on short-axis slices, the myocardium was divided in 36 segments. The maximum number of counts in each segment was calculated. Maximal (max value) and minimal (min value) values were derived. Regional nonuniformity was determined from these values as follows:

$$\text{Regional nonuniformity (RNU \%)} = \frac{\text{max value} - \text{min value}}{\text{max value} + \text{min value}} * 100\%$$

Regional nonuniformity values are presented in this paper as mean value ± 1 s.d. Mean values were determined by averaging five short-axis slices of the phantom.

RESULTS

Circular Orbit—Phantom at the Center of Rotation

The reconstructed short-axis images of a homogeneous cylindrical phantom employing simulated circular orbits with different radii showed *visually* homogeneous count distribution (Fig. 3). Quantitative analysis showed regional nonuniformity ranging from 3.4% to 6% (Fig. 4). However, these values were not significantly different for any of the radii. This nonuniformity error can be explained by normal statistical noise and reconstruction inaccuracies. These data confirm that the proposed simulation model provides data that are free of errors and artifacts. A change in simulation variables (such as the distance of the phantom from the camera) may result in changes in the reconstructed images. These changes will be specific for a variable that was changed. Thus, evaluation of the effect of one variable at a time is possible.

Elliptical Orbit—Phantom at the Center of Rotation

For the elliptical orbits, a significant increase in regional nonuniformity was noted with increasing long-to-short axis ratio. A linear relationship (Fig. 4) existed between the ellipse ratio and regional nonuniformity. The correlation coefficient was 0.98. Regional nonuniformity can be described as:

$$\text{RNU \%} = 17.3\% * \text{R} - 13.7\%,$$

where R equals the long-to-short axis ratio for a given elliptical orbit.

Circular Orbit—Phantom Positioned Out of the Center of Rotation

Simulation of circular orbits but with the phantom placed away from the center of rotation resulted in regional nonuniformity on reconstructed slices. With the increasing distances from the axis of rotation, regional nonuniformity increased. The offset from the center of rotation was expressed as a percentage of the radius of the circular orbit (offset %). As seen in Figure 5, RNU % correlated with offset value with a correlation coefficient equal to 0.99.

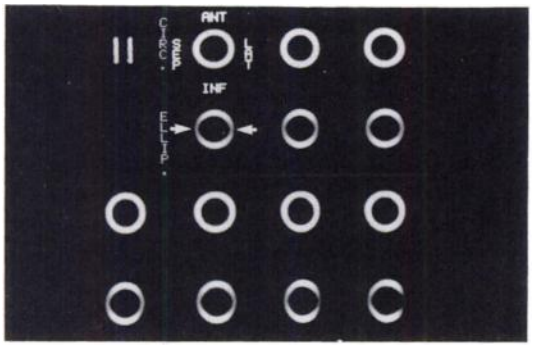

FIGURE 3. Reconstructed short-axis slices of a normal phantom. Top row: simulated circular orbit (CIRC). Bottom row: simulated elliptical orbit (ELLIP), see text. The images acquired with the *circular* orbit show homogeneous distribution of ^{201}Tl. The simulated *elliptical* orbit (long-to-short axis ratio 2:1) results in artifacts (arrows) similar to those seen in patients: 180-degree diametrical defects in ^{201}Tl distribution.

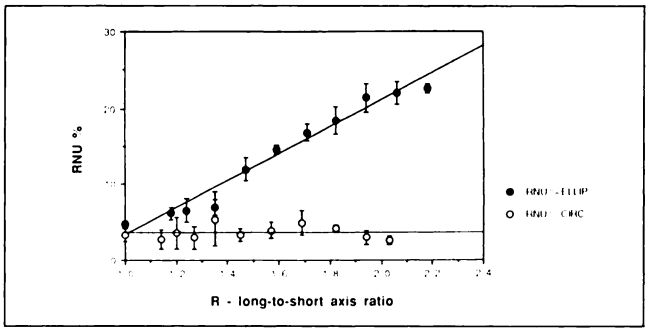

FIGURE 4. Relationship between long-to-short axis ratios (R) of various *elliptical* orbits and measured regional nonuniformity (RNU %) on reconstructed short-axis slices (●). Regional nonuniformity for *circular* orbits with various radii is also displayed (○). The radius of circular orbits was equal to the long-axis of corresponding elliptical orbit.

DISCUSSION

The present study demonstrates that varying distance from the source of activity (i.e, the heart) to the detector can create serious artifacts on ^{201}Tl SPECT images due to varying spatial resolution. Significant regional nonuniformity, as well as distortion of shape was noted on reconstructed images. The artifact due to an elliptical orbit is characteristic and constitutes 180-degree diametrical defects (Fig. 1A).

Although ^{201}Tl SPECT has found widespread use for the evaluation of coronary artery disease, there still remain significant technical challenges with regard to design of instrumentation and data reconstruction.

The design of current tomographic gamma camera systems by necessity is a compromise between image resolu-

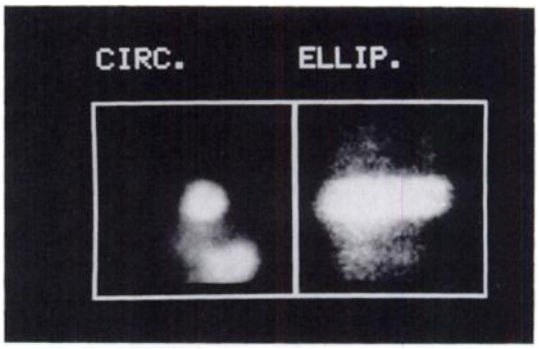

FIGURE 5. Relationship between measured regional nonuniformity (RNU %) and offset value (distance from the center of rotation, calculated as a percentage of radius) for the circular orbit simulation with the phantom out of the center of rotation.

tion and count sensitivity. The relatively low dose of ^{201}Tl, as well as the relatively small fraction of ^{201}Tl accumulated in the heart, results in suboptimal image count density. Consequently, tomographic gamma camera systems are equipped with general all-purpose collimators that have relatively high sensitivity but only fair spatial resolution. Moreover, the spatial resolution of these collimators deteriorates significantly with increasing distance from the target. The latter is relevant for the findings in the present study.

There are two ways in which this may be a significant problem in clinical ^{201}Tl SPECT imaging.

1. Because of the relatively low resolution of typical ^{201}Tl studies, a "body contour" or "peanut" orbit has been proposed. The detector head is brought as close as possible to the heart during a 180-degree rotation. This orbit comprises portions of several elliptical orbits and therefore, depending on the ratio between the long- and short-axis, *artifactual inhomogeneity* of ^{201}Tl distribution may be created.
2. The heart is in an *eccentric* location in the chest. A circular orbit around a patient's body may be in fact an elliptical orbit around the heart. The artifact described in the present study is not seen in all patients. It is conceivable that its presence depends on the patient's size, degree of low energy radiation scatter and attenuation.

In order to avoid artifacts, rotational tomography should be performed with the heart in the center of rotation. This can be easily checked by visual inspection of the cine display of the 32 analog images. If the heart is eccentric, it appears to "run" from one side of the screen to the other. In contrast, when the heart is in the center of rotation, the heart "pivots" in the center of the screen. Figure 6 shows an example of a patient imaged with a body contour orbit and with a circular (around the heart) orbit.

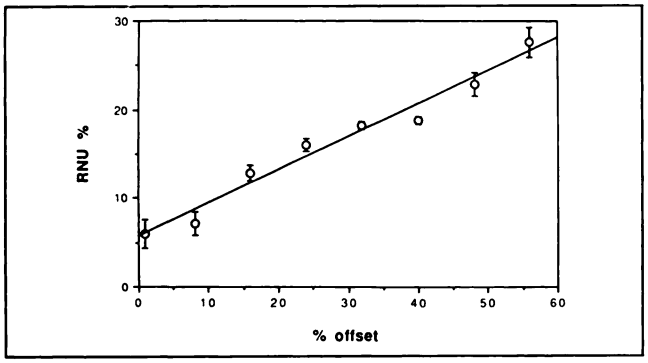

FIGURE 6. Summed planar projections (n = 32) of 180-degree rotation using a *circular* (CIRC.) and *elliptical* (ELLIP.) orbit. Such images can serve as a practical method for evaluating the orbit relative to the heart in a patient study. When the heart is eccentric relative to the center of rotation of the camera, the actual orbit around the heart is elliptical; on cine display the heart will "run" from one side of the screen to the other (right). In contrast, when the heart is in the center of rotation, the heart pivots around its own axis on cine display without much lateral motion (left).

These artifacts may be minimized with the use of technetium-99m-labeled perfusion imaging agents and/or use of multi-head gamma cameras. Both provide considerably better counting statistics and make it feasible to use a high-resolution collimator. Spatial resolution changes less with distance using a high-resolution collimator than with a general, all-purpose, low-resolution collimator. As a result, artifacts will be less prominent.

Some previous studies suggested that degradation of spatial resolution with a distance may be a source of technical problems in positron emission tomography (PET) (*18–20*). Kojima et al. (*21*) demonstrated that finite spatial resolution affects quantitative analysis of SPECT images. Knesaurek et al. (*22*) noted that variation in distance from the collimator may be one of the factors creating geometric distortion in SPECT imaging, in particular when 180-degree rotation is employed.

To improve the resolution of SPECT imaging, several manufacturers introduced noncircular or elliptical orbits. By using such orbits, spatial resolution improved 1–2 mm with no corresponding loss in system sensitivity (*23*). Unfortunately, as shown in the present study, the effect on uniformity is substantial and produces undesirable artifacts. In theory, a 360-degree orbit would demonstrate less nonuniformity due to the averaging effect of opposite views. However, for ^{201}Tl cardiac imaging the dorsal 180-degree data are of inferior quality due to attenuation and have a further major degrading effect on reconstruction.

Implications for Clinical Imaging

In order to minimize the described artifact, we recommend careful positioning of the heart in the center of rotation of a 180-degree circular orbit for rotational tomography. It should be recognized that this modification may cause some loss of spatial resolution by the increased distance from the heart to the camera head. Presently, we are in the process of developing algorithms that automatically will correct for the loss of resolution as a function of distance.

REFERENCES

1. Garcia EV, Van Train K, Maddahi J, et al. Quantification of rotational thallium-201 myocardial tomography. *J Nucl Med* 1985;26:17–26.
2. Tamaki N, Yonekura Y, Mukai T, et al. Stress thallium-201 transaxial emission computed tomography: quantitative versus qualitative analysis for evaluation of coronary artery disease. *J Am Coll Cardiol* 1984;4:1213–1221.
3. Tamaki N, Yonekura Y, Mukai T, et al. Segmental analysis of stress thallium myocardial emission tomography for localization of coronary artery disease. *Eur J Nucl Med* 1984;9:99–104.
4. Maddahi J, Van Train K, Wong C, et al. Quantitative analysis of Tl-201 myocardial single-photon emission computerized rotational tomography: development, validation, and prospective application of an optimized computerized method [Abstract]. *J Am Coll Cardiol* 1986,7:22A.
5. DePasquale E, Nody A, DePuey G, et al. Quantitative rotational thallium tomography for identifying and localizing coronary artery disease. *Circulation* 1988;77:316–327.
6. Starling MR, Dehmer GJ, Lancaster JL, et al. Comparison of quantitative

SPECT vs. planar thallium-201 myocardial scintigraphy for detecting and localizing segmental coronary artery disease [Abstract]. *J Am Coll Cardiol* 1985;5:531.
7. Fintel DJ, Links JM, Brinker JA, Frank TL, Parker M, Becker LC. Improved diagnostic performance of exercise thallium-201 single-photon emission computed tomography over planar imaging in the diagnosis of coronary artery disease: a receiver-operating characteristic analysis. *J Am Coll Cardiol* 1989;13:600–612.
8. Breisblatt WM, Barnes JV, Weiland F, Spaccavento LJ. Incomplete revascularization in multi-vessel percutaneous transluminal coronary angioplasty: the role for stress thallium-201 imaging. *J Am Coll Cardiol* 1988;11:1183–1190.
9. Mahmarian JJ, Boyce TM, Goldberg RK, Cocanougher MK, Roberts R, Verani MS. Quantitative exercise thallium-201 single-photon emission computed tomography for the enhanced diagnosis of ischemic heart disease. *J Am Coll Cardiol* 1990;15:318–329.
10. Tamaki S, Najajima H, Murakami T, Yui Y, Kambara H, Kadota K. Estimation of infarct size by myocardial emission computed tomography with Tl-201 and its relation to creatine kinase-MB release after myocardial infarction in man. *Circulation* 1982;66:994–1001.
11. Ritchie JL, Williams DL, Harp G, Stratton JL, Caldwell JH. Transaxial tomography with thallium-201 for detecting remote myocardial infarction. *Am J Cardiol* 1982;50:1236–1241.
12. Caldwell J, Williams D, Harp G, Stratton J, Ritchie J. Quantitation of size of relative myocardial perfusion defect by single-photon emission computed tomography. *Circulation* 1984;70:1048–1056.
13. Maddahi J, Van Train KF, Wong C, et al. Comparison of thallium-201 SPECT and planar imaging for evaluation of coronary artery disease [Abstract]. *J Nucl Med* 1986;27:999.
14. Friedman J, Berman DS, Van Train K, et al. Patient motion in thallium-201 myocardial SPECT imaging. An easily identified frequent source of artifactual defect. *Clin Nucl Med* 1988;13:321–324.
15. De Pasquale EE, Nody AC, DePuey EG, et al. Quantitative rotational thallium-201 tomography for identifying and localizing coronary artery disease. *Circulation* 1988;77:316–327.
16. DePuey EG, Garcia EV. Optimal specificity in thallium-201 SPECT through recognition of imaging artifacts. *J Nucl Med* 1989;30:441–449.
17. King MA, Penney BC, Glick SJ. An image-dependent Metz filter for nuclear medicine images. *J Nucl Med* 1988;29:1980–1989.
18. Hoffman EJ, Huang SC, Phelps ME. Quantitation in positron emission computed tomography. 1. Effect of object size. *J Comp Assist Tomogr* 1979;3:299–308.
19. Mazziotta JC, Phelps ME, Plummer D, Kuhl DE. Quantitation in positron emission computed tomography. 5. Physical-anatomical effects. *J Comp Assist Tomogr* 1984;8:514–522.
20. Kessler RM, Ellis JR Jr, Eden M. Analysis of emission tomographic scan data: limitations imposed by resolution and background. *J Comp Assist Tomogr* 1984;8:514–522.
21. Kojima A, Matsumato M, Takahaski M, Hirota Y, Yoshida H. Effect of spatial resolution on SPECT quantification values. *J Nucl Med* 1989;30:508–514.
22. Knesaurek K, King MA, Glick SJ, Penney BC. Investigation of causes of geometric distortion in 180° and 360° angular sampling in SPECT. *J Nucl Med* 1989;30:1666–1675.
23. Jaszczak RJ, Coleman RE. Single-photon emission computed tomography (SPECT). Principles and instrumentation. *Invest Radiol* 1985;20:897–910.

EDITORIAL

SPECT and Artifacts—In Search of the Imaginary Lesion

Intelligence . . . is the faculty of making artificial objects. . . .
L'Evolution Créatrice
Henri Bergson, 1907

More than a decade after the introduction of commercial rotating camera SPECT systems it appears that we are still on the toe of the learning curve for this technology. It is a continuing source of amazement that this technique can harbor so many surprises and run so perversely counter to our experience with planar imaging and our hard won intuitions.

Early in our experience with SPECT as a clinical tool, it was learned that the method was technically demanding and fraught with potential traps for the careless practitioner. Statistical noise, which we had learned to deal with as a simple Poisson function that could be easily understood and managed, suddenly loomed as a monster in a new embodiment. The demands for counts skyrocketed (*1*) and noise in these computer-reconstructed images took on a new guise, which sometimes looked disturbingly like real structure. To deal with the noise chimera, we learned we could tailor the filters used in "filtered backprojection" to suit the specific imaging situation. Of course, in so doing, we could also erase real structure and obscure real information.

Artifacts loomed out of the mists of inexperience (*2*). Camera performance suddenly became critically important. Camera field nonuniformities that were not only tolerable but invisible in conventional imaging situations suddenly proved to be intolerable for SPECT (*3,4*). The demands for quality control on SPECT equipment ballooned to a point where some practioners stated, "We can't be bothered doing that sort of thing." After all, spending an hour or more per camera just doing field floods was time wasted and money down the drain. Wasn't it?

Considering the problems with statistical noise that have been emphasized with SPECT, it comes as a real shock to discover that the optimum choice of collimators for SPECT is almost always in favor of higher resolution and *lower* sensitivity. As counterintuitive as this seems, the truth of this fact is supported by mathematical modeling (*5*), simulation experiments (*6*), and practical trials (*7*).

Faced with many seemingly conflicting and counterintuitive facts regarding the technical conduct of SPECT studies, the practitioner is left with little choice but to specify rigid, highly detailed protocols for the conduct of each and every study and to demand that the technologists responsible for conducting these studies follow such protocols unvaringly. Having made such a decision, the problem

Received Jan. 9, 1991; accepted Jan. 29, 1991.
For reprints contact: John W. Keyes, Jr., MD, Division of Nuclear Medicine, Georgetown University Hospital, 3800 Reservoir Rd. NW, Washington, DC 20007.